rich2/zod-osa/zod-osa/zod00206/zod2656-06z | xppws | S=1 | 11/20/05 | Art: LP-62302 | Input-cw-low, cw-mke

Infrared Balloon Experiment: improved instrumental configuration and assessment of instrument performance

G. Bianchini, A. Boscaleri, B. Carli, F. Mencaraglia, L. Palchetti, and E. Pascale

During the 2002 environmental satellite Envisat mid-latitude validation campaign, a new upgraded configuration of the Infrared Balloon Experiment (IBEX) Fourier transform spectrometer, which had its first flight in 1978, performed a stratospheric balloon flight across the Mediterranean Sea. Among the substantial upgrades made to the instrument, the use of photon-noise-limited detectors permitted us to reach the theoretical limits in terms of signal-to-noise ratio. Also, important modifications were made to the interferometric system and electronics, such as the installation of a solid-state laser reference source and an onboard data recording system. During the flight, measurement of volume-mixing-ratio vertical profiles of O_3, HNO_3, N_2O, and ClO from an altitude of ≈38 km were performed with a vertical resolution of ≈1.5 km. © 2006 Optical Society of America

OCIS codes: 300.2140, 300.6270, 300.6300, 280.0280, 010.1280.

AQ: A

1. Introduction

The Infrared Balloon Experiment (IBEX) Fourier transform (FT) spectrometer was designed in the 1970s to perform limb-sounding measurements of the concentration of atmospheric trace species from a stratospheric balloon platform.

The instrument, described in its original design in previous papers,[1–3] is a high-resolution (0.0025 cm^{-1}) polarizing FT spectrometer with two input and two output ports, operating in the far-infrared spectral region from 10 to 250 cm^{-1} and observing atmospheric limb emission near and below the horizontal. A similar version of the flight instrument was also used for laboratory measurements.[4,5] In a few cases laboratory measurements were made in an upgraded mode, either to enhance resolution[6] or to enhance the signal,[7] but none of these possibilities were implemented on the flight instrument.

The instrument was flown several times within the framework of different intercomparison and validation campaigns:

- IBEX campaigns from Palestine, Tex., 1978–1979[8,9]
- Balloon intercomparison campaigns from Palestine, Tex., 1982–1983[10–13]
- Upper-atmosphere research satellite validation campaigns from Fort Sumner, N. Mex., 1993–1994.[14–26]

Within the framework of these campaigns, taking advantage of the possibility of using two detectors to cover different spectral ranges for the two output ports, and through careful choice of the spectral windows, broadband and narrowband, it was possible to collect results related to both the composition of the stratosphere and the vertical distribution of the minor constituents (HCl, HF, HBr, ClO, HCN, CO, and H_2O andO_3 with isotopes).

Recently the instrument was flown from the Italian Space Agency (ASI) launch facility in Trapani-Milo, Sicily, first for a test campaign in July 2000 and then, on 29 July 2002, for a campaign aimed at validating measurements from the Michelson interferometer for passive atmospheric sounding (MIPAS) on board the environmental satellite Envisat.

In view of these campaigns, a major refurbishment of the instrument was performed, including the installation of a diode laser reference source in place of the He–Ne laser, the use of a compact cryogenic detector module, a new onboard data-recording system, and an azimuth control system.

In this paper both an assessment of the new instrument capabilities and the results obtained during the latest Envisat campaign are provided as a summary of this 25 year experience in stratospheric FT

The authors are with the Istituto di Fisica Applicata Nello Carrara, Consiglio Nazionale delle Ricerche, Florence, Italy. L. Palchetti's e-mail address is L.Palchetti@ifac.cnr.it.

Received 23 May 2005; revised 8 September 2005; accepted 8 September 2005.

0003-6935/06/020001-11$15.00/0

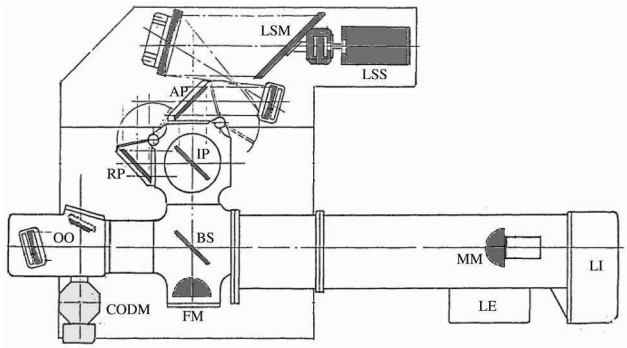

Fig. 1. Schematic of the IBEX optical layout: LSS, limb-scanning system; LSM, limb-scanning mirror; OO, output optics; LI, laser interferometer; LE, laser control electronics.

spectroscopy. In Section 2 a brief description of the instrument in the updated configuration is given. Section 3 gives a description of the instrument performance, and Section 4 gives the results obtained during the Envisat campaign. Finally in Section 5, a brief description of campaign logistics is presented.

2. IBEX Fourier Transform Spectrometer

The IBEX interferometer is based on the polarizing version of the Michelson interferometer, first applied by Martin and Puplett[27] and Martin.[28] The optical layout, which is similar to the one described in previous papers,[1–3] is shown in Fig. 1. With respect to the original version, the only change in the optical design is in the output optics, because the two-detector–two-Dewar system previously used is now superseded by a two-detector–one-Dewar system. Referring to Fig. 1, one of the two arms features moving rooftop mirror MM, which travels over a stroke of ~1 m on a rail guide driven by a linear electromagnetic motor; another fixed rooftop mirror FM is mounted in the other arm. Both the rooftop mirrors are made of gold-plated aluminum on an aluminum sponge substrate to obtain low weight and high stability and have an internal angle of 90° with a specified accuracy of ±10 arc sec. The instrument features two input ports (one input port, AP, is used for the measurement of the atmospheric radiance, and the other, RP, for a reference source) and two output ports, which are enclosed in the cold optics and detector module (CODM). The two input ports are combined by input polarizer IP, and the splitting of the radiation traveling along the two interferometer arms is done by polarizing beam splitter BS. Both IP and BS are wire-grid meshes with 12 μm wire diameter and 25 μm grid pitch. These are effective below 140 cm^{-1}, but photolithographic polarizers on a Mylar substrate with a finer grid can also be used to operate at higher wavenumbers.

In normal operations the two input ports are configured so as to observe atmospheric emission at a direction defined by limb-scan mirror LSM and from a nominal zenith (actually 45° above horizontal). For calibration it is possible to insert temperature-stabilized masks as reference ambient-temperature blackbodies (BBs) in front of either input port.

Table 1. IBEX Fourier Transform Spectrometer Specifications

Instrument type	Polarizing FT spectrometer
Dimensions	300 × 170 × 80 cm
Weight	1000 kg
Interferogram acquisition time	135 s
Observation technique	Limb-sounding emission
Flight altitude	38 km
Field of view	0.3°
Vertical resolution	~1.5 km
Optical channels	2
Spectral range	10–250 cm^{-1}
Spectral resolution	0.0025 cm^{-1}

Beginning in 1998, a new cycle of upgrading of the IBEX spectrometer was started, with the goal of backporting some of the improvements that were implemented in the new spectroscopy of the atmosphere using far-infrared emission/airborne (SAFIRE/A) instrument.[29,30] A summary of the main characteristics of the upgraded IBEX instrument is given in Table 1. Improvements are described in the following subsections.

A. Cold Optics and Detector Module

The CODM, shown in Fig. 2, developed in collabora-

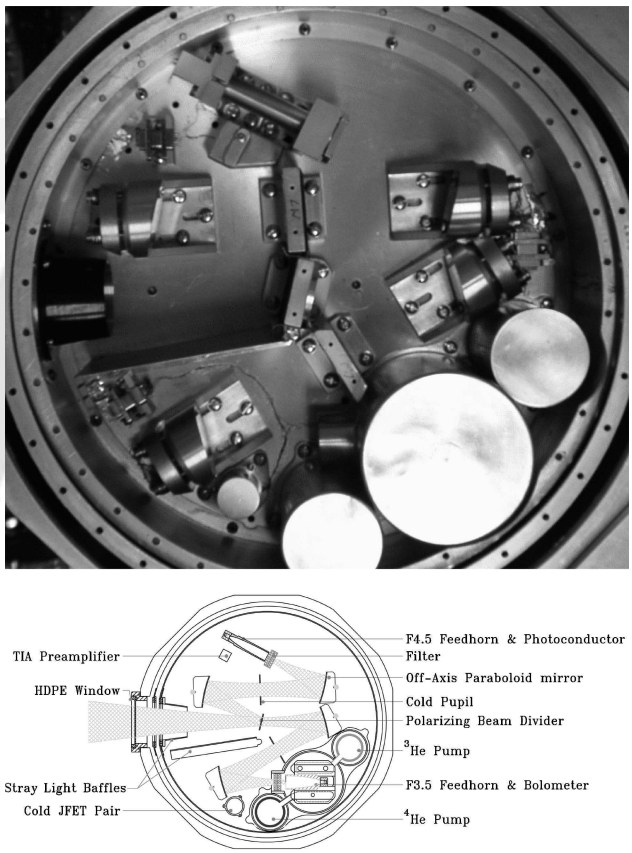

Fig. 2. Photograph and schematic of the cold optics plate inside the CODM. TIA, ●●●; HDPE, ●●●; JFET, ●●●.

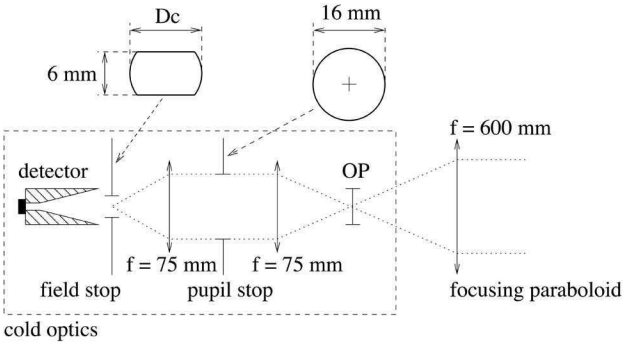

Fig. 3. Optical layout of beam-shaping optics on the cold plate of the CODM. The horizontal field stop (Dc) is adjusted depending on the operating spectral window. An OP separates the two channels.

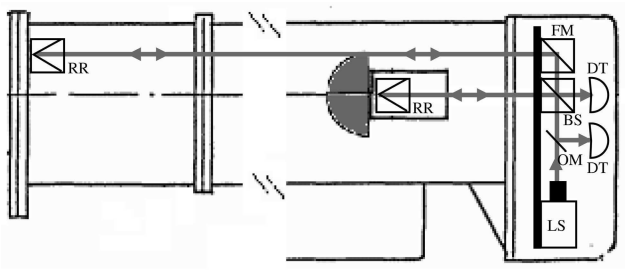

Fig. 4. Optical layout of the reference interferometer used to control the moving mirror system: RR, cube corner retroreflector; FM, folding mirror; OM, output mirror; LS, laser source; DT, photodiode detectors.

tion with Queen Mary and Westfield College (London), encloses output optics, including pupils and field stops, the output polarizer (OP), bandpass filters and collecting optics, and the two detectors corresponding to the two acquisition channels. The OP is a photolithographically deposed wire grid on a 1.5 μm Mylar substrate. The wire thickness is 1 μm, and the wire-grid pitch is 2 μm. The two detectors are of different types: a photoconductive detector operating at 4 K covering spectral intervals, extending from 50 to 250 cm^{-1}, and a bolometric detector operating at 0.3 K, covering the 10–50 cm^{-1} region. A narrowband may be selected for each detector by use of suitable bandpass filters inserted in the cold part of the system. The bolometric detector is cooled through an additional closed-circuit ^{3}He cooling stage mounted on the cold plate of the cryostat. This setup allows the full exploitation of photon-noise-limited detectors. In F3 Fig. 3 a simplified schematic of the beam-shaping optics mounted on the cryostat cold plate is shown. The vertical aperture of the field stop gives a beam divergence of ~0.6° inside the instrument, which, considering the 2:1 input telescope, gives an atmospheric vertical field of view of ~0.3°, for an average vertical resolution of ~1.5 km. The throughput of the system varies from 1.1×10^{-6} to 2.0×10^{-6} m^2 sr, depending on field-stop horizontal aperture Dc, which is adjusted to match the working wavenumber of the detector. The characteristics of the narrowband filters used on the IBEX instrument are given in T2 Table 2. Along with the line center and bandwidth, the table also shows the corresponding field-stop horizontal aperture and the chemical species whose spectral lines are present inside the filter band.

Table 2. Narrowband Filters Used in the IBEX Spectrometer for Selecting the Operating Spectral Region

Center Wavenumber (cm^{-1})	Bandwidth (cm^{-1})	Chemical Species	Field-Stop Width[a] (mm)
23	1	O_3, ClO, N_2O, HNO_3	15
118	2	H_2O, OH, HOCl, O_3	6.7

[a]The maximum field-stop width permitted depends on the center wavenumber of the filter.

B. Diode Laser

The position of the carriage is controlled by measuring fringes of a laser interferometer that has the MM mounted on the back of the infrared scanning mirror, as shown in Fig. 4. The two output ports of this interferometer are spatially separated, and a special absorbing BS causes the two outputs to be 90° out of phase instead of the standard 180°. This allows us to detect the movement direction and to have a linear resolution of λ/4, where λ is the control-laser wavelength. The control laser, originally a frequency-stabilized He–Ne, is now a diode laser[31] operating in the near infrared at ~780 nm. F4

C. Data Recording

The data flow is sent to downlink the telemetry stream so that both interferogram and housekeeping information can be controlled by the experimenter, making it possible to send commands that depend on the instrument status. Because of the long distance traveled by the balloon, from Sicily to Spain, two down-range facilities were set up in different locations for recording telemetered data, and two telemetering systems (one of which was still in the experimental stage) were mounted on the gondola. An added security transmission was made more robust against telemetry errors by passing data through a Viterbi encoder[32] before sending the data, and a redundant recording system was installed on board the instrument, storing on a hard disk all the acquired data.

D. Attitude Control System

The attitude control system has two main parts: the azimuth control and the elevation control.

IBEX, designed to draw the vertical profiles of minor atmospheric constituents, needs a relatively low accuracy (around 5°) in azimuth coordinate reconstruction, and a low-cost two-axis magnetometer is the best absolute position sensor for driving all the heading movements. The azimuth control loop, built outside the experiment, is made of a mechanical part (pivot) and an electronic part.[33–35] The first one is

located at the interconnecting point between balloon and gondola and is used to rotate the payload to either point to or scan a given sky target, and to compensate for the disturbance torque coming from the random rotation of the balloon when in staring mode. The pivot mechanical design was stress analyzed according to the safety statement suggested by NASA's National Scientific Balloon Facility (10 G vertical and 5 G at 45°). The actual pivot design is capable of driving a payload up to 2500 kg of total weight. The electronic part of the azimuth control system is based on a CPU subsystem and has the goal of interfacing the onboard telemetry system, reading the sensors, supplying power to the motor, and sending data to both the radio links and the onboard backup data storage.

An accurate elevation control is needed for limb-sounding measurements. The pointing is controlled by a single-axis platform (SAP) designed and built by the Smithsonian Astrophysical Observatory (SAO).[36,37] The system gives a mechanical vertical reference relative to which the elevation mirror performs the limb-scan stabilization with a nominal accuracy of approximately ±0.01°.

E. Calibration Sources

In early flights, Eccosorb sheets, Model AN-72, were used as an ambient-temperature reference source in the two input ports. In more recent flights, Eccosorb, Model CR-114, was used because, even if its blackness is lower than that of the AN-72 (reflectivity ≤10%), it has higher thermal conductivity and ensures a more homogeneous surface temperature. The undesired effect of polarization[38] may be neglected because the mask is observed at normal incidence. The deviation from blackness is made negligible by the fact that these sources are used at ambient temperature.

3. Instrument Performance

Operative data acquired during flights, even if primarily finalized to atmospheric measurements, were also useful for the characterization of the instrument performance. The following subsections are devoted to the characterization of the main subsystems with data acquired during the last two flights from Sicily to verify the most recent updates.

A. Carriage Movement

As explained in the original paper,[1] the instrument operates in a continuous scanning mode. Stability of the speed is then a strict requirement for avoiding mixing of the frequencies and loss of spectral accuracy.[39,40] A second requirement, which is a general property of all FT spectrometers, is the accuracy in evaluating the mirror position because samples must be taken at equal steps. As pointed out above, the sampling is done at equally spaced intervals that are a multiple n of $\delta = \lambda_{laser}/4$, where λ_{laser} is the wavelength of the controlling laser. The n value depends on the upper frequency of the spectrometer range. In our case the upper frequency $\nu_{max} \sim 250\ cm^{-1}$ dictated a value of 80 for n, leading to an optical Nyquist frequency of $\sim 320\ cm^{-1}$.

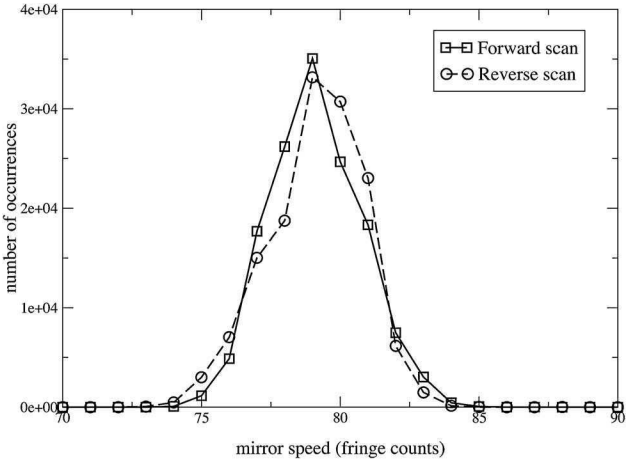

Fig. 5. Speed distribution of the MM system (number of occurrencies in a single scan versus speed value in terms of fringe counts).

The observed distribution of speed, measured in terms of number of δ intervals detected in a constant time interval for forward and reverse movement, is shown in Fig. 5, in good agreement with what was directly measured during laboratory tests, approximately ±3%. Note the difference between the forward and the reverse scanning direction, which has its counterpart in the different currents drawn by the motor in the forward and the reverse mode. The difference between forward and reverse movement is due to small deviations from the horizontal in the direction parallel to the linear motor caused by the change in the position of the MM itself. As shown in Fig. 6 (upper and middle panels), the oscillation measured by inclinometer 1 is correlated with the forward and reverse movements of the MM. Further details on movement characterization may be found in Ref. 41.

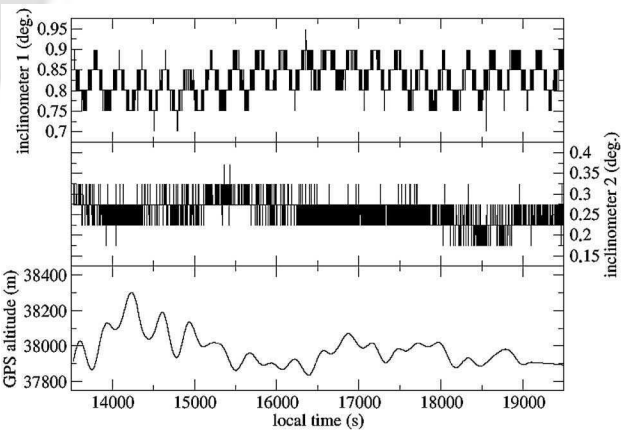

Fig. 6. Instrument attitude data during flight: inclinometer data in directions parallel (upper panel) and perpendicular (middle panel) to the MM guide, and floating altitude (lower panel).

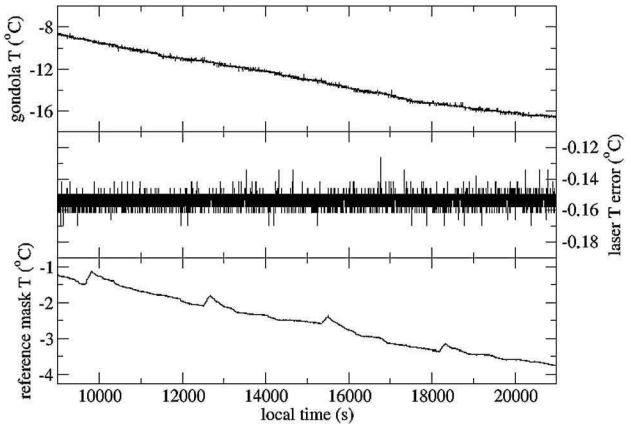

Fig. 7. Temperatures during flight: gondola temperature (upper panel), laser temperature error (middle panel), and reference mask temperature (lower panel).

B. Laser Stability

Stability of the movement and sampling throughout the flight, i.e., frequency stability of the spectrometer, requires stability of the wavelength of the controlling laser, and, in turn, this requires high stability of its temperature. Both an active Peltier system and passive protection by thermal insulation were adopted to minimize external effects such as day–night thermal excursion and changes in the solar thermal load during the day. These precautions proved to work correctly; a stability of the order of a few degrees millikelvin was obtained without any detectable long-term trend, as shown in Fig. 7 (upper and middle panels). Stability of the laser system in the final product was checked to evaluate the position of a narrow atmospheric line measured during calibration spectra obtained looking toward the zenith. The results in Fig. 8 show a frequency fluctuation inside the experimental error and of the order of a few parts in 10^{-4} cm^{-1}, i.e., well below instrumental resolution.

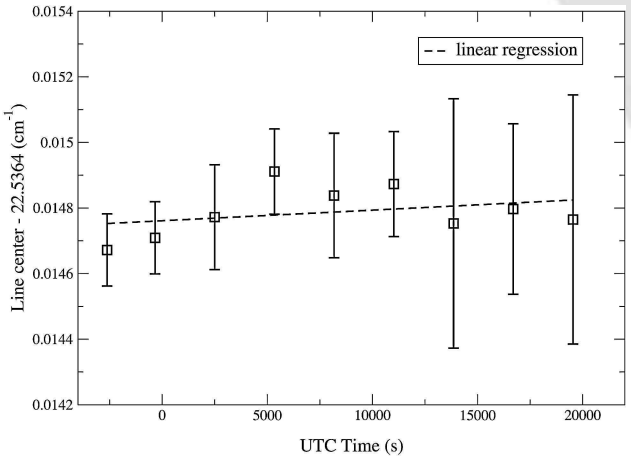

Fig. 8. Frequency stability of the reference laser source estimated from the position of an atmospheric line at 22.5364 cm^{-1}.

C. Reference Temperature

In-flight calibration is done by the insertion, in the field of view, of an Eccosorb mask (see Subsection 2.E). Because of changes in the radiative environment, the mask temperature increases when it is inserted for calibration in front of the warm instrument [see Fig. 7 (lower panel)] and generally decreases slowly when removed and located in a position that looks at the cold environment of the gondola. Because of this thermal drift, a stringent requirement was placed on the thermal conductivity of the observing material so that uniform temperature could be ensured. For data analysis the average temperature of the reference mask during the interferogram acquisition was used.

D. Flight Altitude Stability

Given an angular distance from the zenith, the observed air mass changes depending on balloon height. To compare profiles taken at different times, it is therefore important to keep the float altitude as constant as possible. Height evaluation in former flights was obtained from pressure–temperature profiles and, in a few cases, a calibration was made possible by radar measurements. A more accurate estimation is now possible by use of global positioning system (GPS) sensors. Limited here to the last flight, the float altitude was kept constant within ± 150 m, as shown in Fig. 6 (lower panel), which shows the GPS altitude immediately after the 38 km floating altitude was reached. Slow oscillations are related to atmospheric gravity waves. The power spectrum of these oscillations peaks at ≈ 0.003 Hz corresponds to a period of 5 min. This value is comparable with the time required for the acquisition of a single interferogram ($\sim$2 min), but because of the low amplitude of the oscillations with respect to the vertical resolution (see Section 2), no problems are expected from the vertical motion of the platform during a scan. Both the period and the amplitude of the altitude oscillations are in good agreement with what is expected for the gravity waves in the stratosphere.

E. Azimuth Stability

Accuracy and stability requirements of the azimuth-pointing system, described in Subsection 2.D, come mainly from the following two sources:

- A fast change of the azimuth causes errors in the stability of the line-of-sight position with respect to the vertical.[36,37]
- Uncertainty in the azimuth causes mixing of emission from layers at different solar times, particularly important at sunset and sunrise for molecules whose concentrations depend on photochemical effects (for instance ClO); in this case it is required for observation along the terminator whose angular distance from the local meridian depends on the date and latitude.

Calibration of the local magnetic declination of the system was done at ground with the polar star as

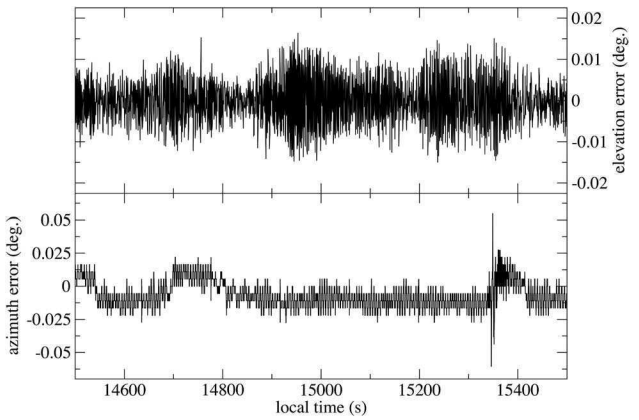

Fig. 9. Pointing accuracy of the instrument: limb-pointing error (upper panel) and azimuth-pointing error (lower panel).

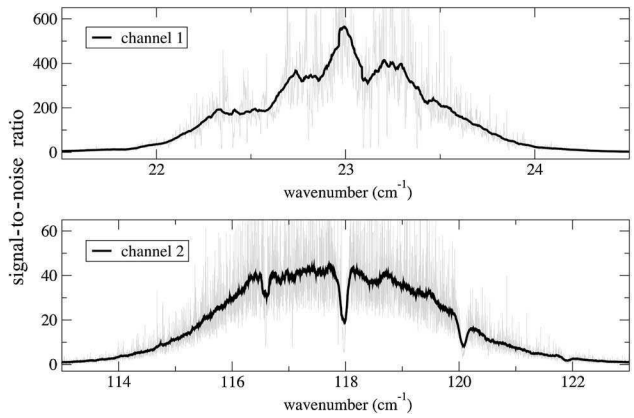

Fig. 10. Instrumental signal-to-noise ratio for the bolometer channel 1 (upper panel) and the photoconductor channel 2 (lower panel).

reference. No correction was made during the flight for the variation in local magnetic declination, expected to be ≈2°. Pointing errors, as measured by the servo, are shown in Fig. 9. It is interesting to note that there is a correspondence between the position of the peak in the spectrum of the azimuth error signal and the frequency expected for a pendulum with a length defined by the distance between the balloon and the payload. In fact, the magnetometer, which is bolted to the gondola frame, experiences a change in magnetic field because of gondola oscillation and therefore corrects for it.

F. Elevation-Angle Stability

Stability of the elevation angle is a primary requisite for the retrieval of vertical concentration profiles, so bench tests were made before each flight with an oscillating plate for which both amplitude and period could be adjusted. No degradation of the performance has been observed since the first use of the SAP. A rms error of ≈1 arcmin has consistently been found in laboratory tests for oscillations as large as 3°, the maximum allowed value for the control to work correctly. Because of the impossibility of repeating on the bench the flight conditions (for instance the main pendulum oscillation), the final proof of correct working may be obtained only by careful inspection of the in-flight data. Stability of the pointing during any scan, estimated from the error signal of servoloops, was kept within the expected value of ≈±0.01°, as shown in Fig. 9. The small oscillations around the required position are, as expected, correlated with the azimuth control error.

G. Detector System

The new CODM deployed in the latest flights allowed us to obtain the best performance measured for this instrument. It uses different detectors for the two spectral channels: a bolometric detector for the 23 cm^{-1} region (channel 1) and a photoconductor for the 118 cm^{-1} region (channel 2). The characterization was performed by measurement of, for the two channels the noise-equivalent spectral radiance (NESR) that gives the overall radiometric performance of the instrument and the time response that affects the noise caused by sampling errors.

The NESR was calculated with a subset of measurements performed during the 2002 flight with the input looking toward the sky at 45° elevation (upward-looking calibration spectra). For this line of sight, spectral features that are due to atmospheric emission have a negligible contribution and measurements are sufficiently stable to calculate the rms value of the acquired spectra. The results give, for each spectral element at 0.0025 cm^{-1}, a NESR of ~0.3 nW/cm^2 sr cm^{-1} for the 23 cm^{-1} channel and ~55 nW/cm^2 sr cm^{-1} for the 118 cm^{-1} channel. The corresponding signal-to-noise ratio (SNR) measured for the limb observation of the atmosphere is shown in Fig. 10. The figure also shows the bandwidth covered by the filters used for the two spectroscopic channels.

The time response was characterized in the laboratory by measurement of the transfer functions of the detector system, which includes the detector and its preamplifier, and of the analog electronic unit (AEU), which conditions the signals before analog-to-digital conversion. In the nominal range of 20–2000 Hz, both systems show a linear phase that corresponds to a constant time delay. The delay is equal to 760 μs for the bolometer channel and 150 μs for the photoconductor; for the AEU, which implements a Bessel filter, the delay is 1600 μs. These delays are compensated for by the introduction of a common constant time delay in the acquisition strobe of 1820 μs. In such a way, the spectral noise that is due to the sampling error can be minimized[42,43] and becomes negligible with respect to the total measurement noise.

H. Instrumental Response Function

The instrumental line shape (ILS) was estimated by use of narrow atmospheric lines found in upward-looking calibration spectra. Because even in this case the linewidth is of the same order of magnitude as

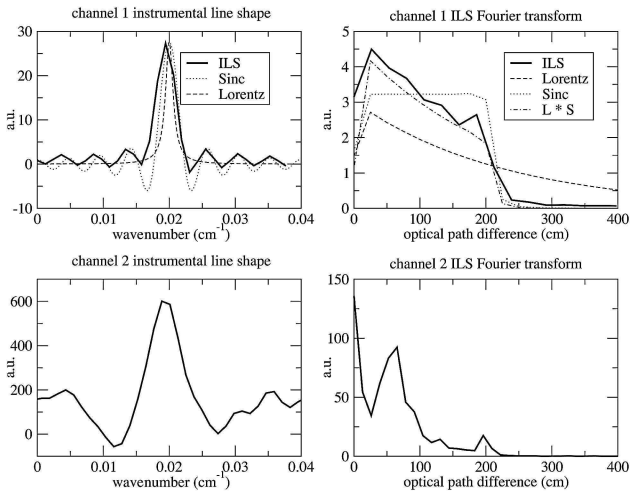

Fig. 11. ILS and its FT for both channels. Theoretical contributions to the ILS are also shown in the long-wavelength case.

that of the theoretical instrumental resolution, we must include in the measured line shape a Lorentzian contribution.

F11 In Fig. 11 the result of an ILS analysis for both channels is shown. The low-frequency channel exhibited a behavior near to that of theoretical predictions: The measured line shape is a convolution of a Lorentz function of the width expected for atmospheric lines at balloon altitude and the sinc function of the theoretical ILS for a FT spectrometer with a 0.0025 cm^{-1} resolution.

The FT of the ILS, also shown in Fig. 11, indicates possible self-apodization effects deriving from a path-difference-dependent misalignment that is due to imperfections in the MM drive[41] that are visible in only the high-frequency channel because of the greater sensitivity to optical alignment of the 118 cm^{-1} channel 2 with respect to the 23 cm^{-1} channel 1. Whereas in the low-frequency channel the FT of the ILS clearly shows a boxcar contribution exactly corresponding to the 200 cm scan length, in channel 2 a substantial decrease of the ILS transform is clearly visible between 100 and 200 cm of scan length. This, as discussed in a previous work,[41] is interpreted as the effect of errors in the mirror movement that affect instrument alignment during a scan. As a consequence, the effective spectral resolution obtained for channel 2 is approximately a factor of 2 lower than that for channel 1.

4. Measurements and Results

The observation strategy adopted by the IBEX instrument is based on limb-scanning sequences consisting of 20 acquisitions, including calibrations. During each sequence the atmosphere is vertically sampled at angular increments of 0.3°, i.e., the vertical field of view of the instrument, thus avoiding oversampling of the line of sight. The vertical resolution depends on the elevation angle and varies from ~1 km in the stratosphere to more than 2 km in the tropopause.

The acquisition time for a complete sequence is approximately 45 min. Considering an average platform ground speed of ~80 km/h, as estimated from GPS data, we obtain a horizontal resolution of ~60 km, corresponding at a latitude of 38° to ~0.7° of longitude.

The data-retrieval process is usually split into two phases, the first (level 1) giving calibrated atmospheric emission spectra and the second (level 2) performing the retrieval from limb sequences of calibrated spectra to vertical profiles of atmospheric constituents.

A. Level 1: From Interferograms to Calibrated Atmospheric Emission Spectra

The Level 1 analysis was performed with the following sequence of operations:

1. Interferogram handling, which includes

- correction of spurious effects such as cosmic-ray spikes,[44]
- phase-error correction of the interferogram,
- FT of the interferogram;

2. spectrum calibration, which includes

- subtraction of the instrumental background, as measured with zenith view,
- spectral calibration by use of BB measurements,
- frequency calibration by use of known atmospheric lines.

In-flight calibration of the instrument is ensured by the availability of two input ports and two output ports that receive different linear combinations of the input signals. In standard operating conditions the instrument observes the atmosphere in input port AP and the reference BB mask in input port RP (measurement M1). One makes the in-flight calibration by setting the line of sight at a high elevation angle (+45°, measurement M2) and by inserting a second BB mask at known temperature in front of the AP port (measurement M3).

As a first approximation we can assume that emission measured well above horizontal is negligible, so the responsivity of the instrument may be retrieved from two measurements (M2, M3). Because in measurement M3 the two masks have similar temperatures, from this measurement we obtain a measurement of the instrument self-interferogram.[45]

An example of measured spectra for a typical limb-scanning sequence is shown in Fig. 12. For the sake F12 of simplicity a subset of the 18 different observation angles is shown.

B. Level 2: From Spectra to Profiles

In the IBEX campaigns before 1982, data analysis was focused on line assignments, i.e., recognizing the presence of different components in the atmospheric emission.[8,9,46] Development of forward mod-

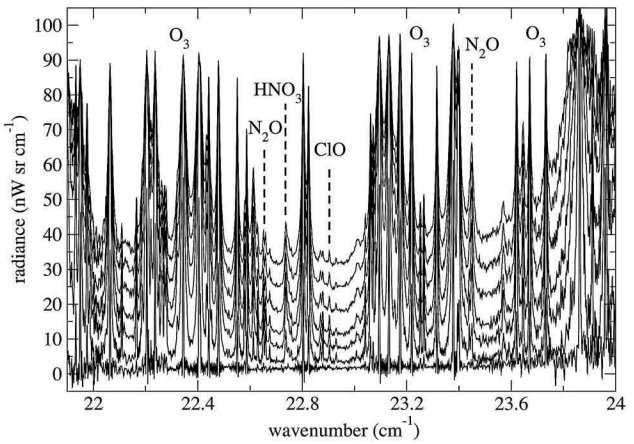

Fig. 12. Sequence of spectra acquired at different elevation angles in the 23 cm^{-1} spectral window (channel 1). Not all the elevation angles included in the sequence are shown. Relevant spectral features from atmospheric trace gases are evidenced.

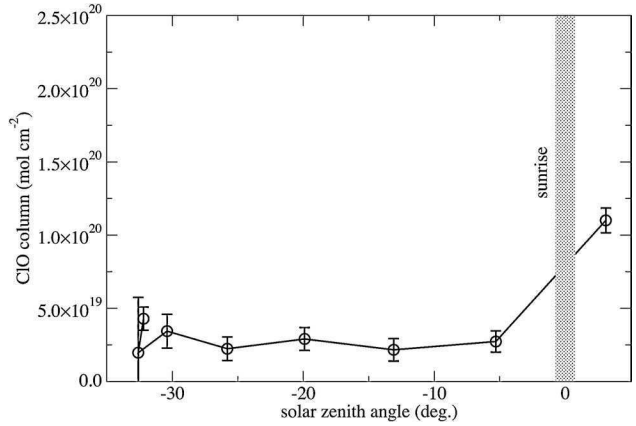

Fig. 14. ClO column content in successive limb-scanning sequences. The sudden increase in concentration is strictly correlated with the sunrise time (corrected for balloon height).

els and retrieval algorithms[47–50] since then has allowed the retrieval of vertical distribution of the minor atmospheric constituents. The availability of high-performance detectors coupled with the high efficiency of the instrument and sophisticated retrieval techniques makes it possible to exploit even very small signals. As an example we show in Fig. 13 the ClO vertical-distribution profiles measured during the 2002 flight (each profile corresponds to a single sequence), and in Fig. 14 the column density for ClO versus time. The timing of the sudden increase is in excellent correspondence with the sunrise time corrected for the balloon altitude. Note that in the earlier measurements the observation of ClO required averaging over several sequences,[16] whereas in the current data diurnal variations can be estimated from single profiles.

In Fig. 15 vertical distribution profiles of other measured species (ozone, nitrous oxide, and nitric acid) are shown. The profiles are obtained from an

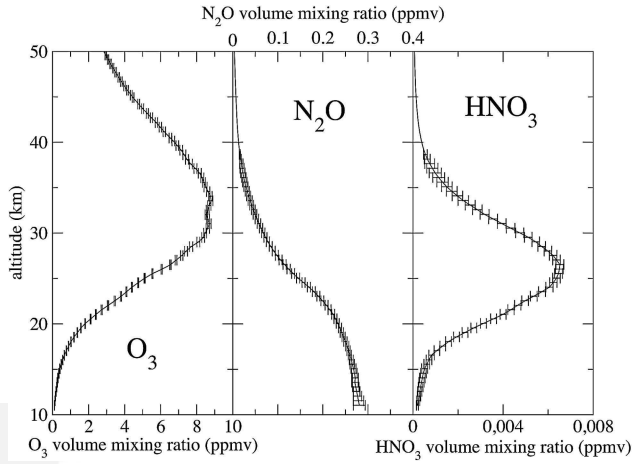

Fig. 15. Vertical-distribution profiles retrieved from a single limb-scanning sequence for ozone, nitrous oxide, and nitric acid.

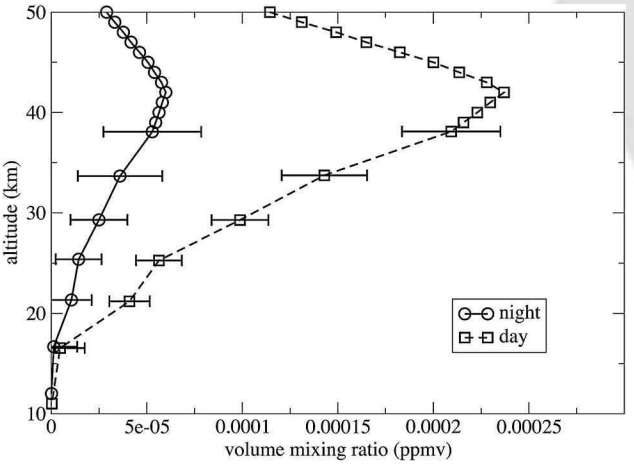

Fig. 13. Two ClO profiles retrieved from different limb-scanning sequences before and after sunrise. The diurnal cycle of ClO is clearly evident from single sequences.

average of eight limb-scanning sequences acquired at a floating altitude of 38 km. Retrieval errors for a single sequence are of the order of 1% for O_3, 2% for N_2O, and 5% for HNO_3 calculated at the peak of concentration. Systematic retrieval errors that are due to atmospheric modeling are expected to be of the same magnitude as was estimated for HNO_3.[51]

Retrieval results are considerably better than in the old version of the instrument, both in terms of vertical resolution and of concentration errors. This is mainly due to the increased performance of detectors, the better resolution, and the better correction and knowledge of the line of sight. Similar results were reported for other balloonborne FT instrumentation currently used for atmospheric measurements in different spectral regions, such as the balloon version of MIPAS[52] and the infrared atmospheric-sounding interferometer[53] and the SAO far-infrared spectrometer, FIRS-2.[54]

5. Campaign Logistics

Until the 1990s flights all campaigns were done in close cooperation with NASA (Jet Propulsion Laboratory and Langley Research Center). For the initial campaigns, telemetry and data recording were provided by NASA staff. Availability of new funding and of new technology later allowed the use of more compact ground-support equipment. For the latest flights, all controls, including quick look and command sending, were built around two PCs running Linux.

The 2002 Envisat validation flight took place from the ASI facility located in Trapani-Milo, Sicily. The base can launch stratospheric balloons of up to 10^6 m^3 over trans-Mediterranean flights ending over Spain. An international agreement with the Arenosillo base in Spain guarantees recovery of the package. The data–command link relays to the base either directly, when the platform is within telemetry range, or by down-range stations in Spain, one in Mallorca and the other at the Arenosillo base. The operational window of the base is June–July, and this was appropriate for the Envisat validation during the summer season. (On U.S. bases in Palestine, Tex., and Fort Sumner, N. Mex., launches are available during the spring and autumn turnaround.)

AQ: E Validation of satellite data requires that measurements be made over the same air mass and at the same time as the satellite ones. Envisat flies in a Sun-synchronous polar orbit at ~800 km altitude with a repeat cycle of the reference orbit equal to 20 days. The Earth projection of satellite shifts by ~400 km westward between successive passages. The overpass between balloon and satellite requires strict timing because the balloon platform is also moving at a speed that depends on atmospheric conditions (high-altitude wind). A simulation made by the weather forecast services at the ASI base showed that a spatial coincidence of better than 1° of latitude could be achieved, provided weather conditions allowed a launch in the desired time window.

The balloon position is measured by a GPS, and it is possible to change the azimuth observation angle to have the air mass observed by satellite and by balloon as closely as possible. Note that a complete limb-scanning sequence to measure a single vertical profile requires ~45 min for the IBEX instrument, whereas only ~80 s are required for the MIPAS instrument. Any correlation between results obtained by the two instruments assumes that time constants for atmospheric changes are longer than 1 h.

6. Final Remarks

Scientific instruments built around carefully designed elements may be used to produce important results throughout a long time span. This has the advantage of making possible comparison of measurements over long periods and eventually an intercomparison between instruments whose measurement periods do not overlap. This possibility is relevant for atmospheric studies when the bulk of measurements made by different satellites launched in different periods (let us recall the Television Infrared Observation Satellite, the European Remote-Sensing Satellite 2, and the Upper Atmosphere Research Satellite) are indirectly comparable only through the validations done by ground-based or aircraftborne–balloonborne instrumentation. A few instruments that have been operating in the field for several decades (the University of Denver FT spectrometer and the Meteorological Service of Canada FT spectrometer, to name just a couple[55]) are therefore of great importance in filling the gaps between satellite measurements.

In this paper we have described how the IBEX instrument has been used for more than 20 years for field measurements, and a similar instrument was used for laboratory measurements, with several cycles of upgrades when better technologies became available. The last flight, which took place in 2002 within the framework of the MIPAS–Envisat validation was successful not only from the validation point of view, but it has also shown that all updates were working correctly and that the unmodified parts did not show signals of deterioration.

Unfortunately, after this flight, the instrument, recovered in good shape on the Sierra Nevada mountains, was destroyed on its way back to Italy because of a fire on the trailer that was carrying it. A funding request has been made to the ASI to rebuild a similar instrument; it should be noted, in fact, that, after the loss of the IBEX instrument, no limb-sounding spectrometers that operate in the 10–100 cm^{-1} spectral range are available any longer in the worldwide scientific community.

It is almost impossible to acknowledge all the contributions to the successful 20-year-long history of the IBEX instrument. Financial support came mostly from ASI, but important contributions also came from different sources to support more specific activities: The Chemical Manufacturers Association provided a grant for the single-axis platform, the Methil Bromide Coalition partially supported campaigns for the measurement of stratospheric HBr and the European Community partially supported campaigns for cross-validation measurements. Scientific cooperation for both measurements and data analysis has been done with two groups from Bologna: the University of Bologna with M. Carlotti and the Consiglio Nazionale delle Ricerche with B. M. Dinelli; the Queen Mary and Westfield College of London with P. A. R. Ade and C. Lee; and the Oregon University and NASA Langley Research Center with J. M. Russell III, J. H. Park, I. G. Nolt, M. D. Vanek, and the late J. V. Radostiz.

Technical support was provided for the launch from the Italian base in Trapani-Milo, Sicily, by the ASI staff and for the recovery by the Spanish staff in Arenosillo. Finally we acknowledge the contributions of A. Bonetti from the University of Florence, A. Vatteroni from Microdata Due S. r. l., and all people working at the Istituto di Ricerca sulle Onde Elettromagnetiche (now the Istituto di Fisica Applicata

Nello Carrara) who have been working on the project: M. G. Baldecchi, M. Poggesi, D. Tirelli, M. Trambusti, G. Valmori, and V. Venturi.

References

1. B. Carli, F. Mencaraglia, and A. Bonetti, "Submillimiter high-resolution FT spectrometer for atmospheric studies," Appl. Opt. **23,** 2594–2603 (1984).
2. B. Carli, "High resolution far infrared FT spectroscopy of the stratosphere: optimization of the optical design of the instrument," in *1985 International Conference on Fourier and Computerized Spectroscopy*, Proc. SPIE **553,** 93–98 (1985).
3. F. Mencaraglia, B. Carli, A. Bonetti, P. Ciarpallini, M. Carlotti, G. Lepri, F. Alboni, U. Cortesi, and M. Ridolfi, "Stratospheric composition from balloon based measurements," in *Atmospheric Sensing and Modeling*, Proc. SPIE **2311,** 240–247 (1994).
4. B. Carli, M. Carlotti, F. Mencaraglia, and E. Rossi, "Far-infrared high-resolution Fourier transform spectrometer," Appl. Opt. **26,** 3818–3822 (1987).
5. A. Bonetti, E. Rossi, B. Carli, M. Carlotti, G. Di Lonardo, A. Trombetti, and F. Mencaraglia, "Far infrared spectroscopy with a 4-meter path difference interferometer," in *1985 International Conference on Fourier and Computerized Spectroscopy*, Proc. SPIE **553,** 326–327 (1985).
6. B. Carli and F. Mencaraglia, "Twofold Martin–Puplett interferometer," Int. J. Infrared Millim. Waves **2,** 87–96 (1981).
7. B. Carli and F. Mencaraglia, "Signal doubling in the Martin-Puplett interferometer," Int. J. Infrared Millim. Waves **2,** 1045–1051 (1981).
8. M. G. Baldecchi, B. Carli, F. Mencaraglia, A. Bonetti, and M. Carlotti, "Atlas of stratospheric submillimeter lines: the 7–20 cm^{-1} interval," J. Geophys. Res. **89,** 11689–11704 (1984).
9. M. G. Baldecchi, B. Carli, F. Mencaraglia, A. Barbis, A. Bonetti, and M. Carlotti, "Atlas of stratospheric submillimeter lines: the 20–40 cm^{-1} interval," J. Geophys. Res. **93,** 5303–5318 (1988).
10. C. B. Farmer, B. Carli, A. Bonetti, M. Carlotti, B. M. Dinelli, H. Fast, W. F. J. Evans, N. Luisnard, C. Alamichel, D. W. Johnson, W. A. Traub, K. V. Chance, R. Zander, G. Roland, and L. Delbouille, "Balloon intercomparison campaigns: results of remote sensing measurements of HCl," J. Atmos. Chem. **10,** 237–272 (1990).
11. W. G. Mankin, M. T. Coffey, K. V. Chance, W. A. Traub, B. Carli, F. Mencaraglia, S. Piccioli, I. G. Nolt, J. V. Radostitz, R. Zander, G. Roland, D. W. Johnson, G. M. Stokes, C. B. Farmer, and R. K. Seals, "Intercomparison of measurements of stratospheric hydrogen fluoride," J. Atmos. Chem. **10,** 219–236 (1990).
12. D. Murcray, A. Goldman, J. Kosters, R. Zander, W. Evans, M. Luisnard, C. Alamichel, M. Bangham, S. Pollit, B. Carli, B. M. Dinelli, S. Piccioli, A. Valboni, W. A. Traub, and K. V. Chance, "Intercomparison of stratospheric water vapour profiles obtained during the balloon intercomparison campaign," J. Atmos. Chem. **10,** 149–179 (1990).
13. M. G. Baldecchi, A. Barbis, A. Bonetti, B. Carli, M. Carlotti, B. M. Dinelli, F. Mencaraglia, M. Poggesi, E. Rossi, and M. Trambusti, "High-resolution far-infrared FT spectroscopy of the stratosphere," Rend. Fis. Acc. Lincei **6,** 95–110 (1995).
14. I. G. Nolt, P. A. R. Ade, F. Alboni, B. Carli, M. Carlotti, U. Cortesi, M. Epifani, M. J. Griffin, P. A. Hamilton, C. Lee, G. Lepri, F. Mencaraglia, A. G. Murray, J. H. Park, K. Parki, P. Raspollini, M. Ridolfi, and M. D. Vanek, "Stratospheric HBr concentration profile obtained from far infrared emission spectroscopy," Geophys. Res. Lett. **24,** 281–284 (1987).
15. J. H. Park, B. Carli, and A. Barbis, "Stratospheric HBr mixing ratio obtained from far infrared emission spectra," Geophys. Res. Lett. **16,** 787–790 (1989).
16. B. Carli, F. Mencaraglia, M. Carlotti, B. M. Dinelli, and I. G. Nolt, "Submillimeter measurements of stratospheric chlorine monoxide," J. Geophys. Res. **93,** 7063–7068 (1987).
17. M. M. , J. Guo, B. Carli, F. AbbasMencaraglia, A. Bonetti, M. Carlotti, and I. G. Nolt, "Stratospheric O_3, H_2O and HDO distribution from balloon based far infrared observations," J. Geophys. Res. **92,** 8354–8364 (1987).
18. B. Carli, M. Carlotti, B. M. Dinelli, F. Mencaraglia, and J. H. Park, "The mixing ratio of the stratospheric hydroxil radical from far infrared emission measurements," J. Geophys. Res. **94,** 11049–11058 (1989).
19. M. Carlotti, P. A. R. Ade, B. Carli, M. Chipperfield, P. A. Hamilton, F. Mencaraglia, I. G. Nolt, and M. Ridolfi, "Diurnal variability and night detection of stratospheric hydroxil radical from far infrared emission measurements," J. Atmos. Solar-Terr. Phys. **63,** 1509–1528 (2001).
20. B. Carli and J. H. Park, "Simultaneous measurements of minor stratospheric constituents with emission far infrared spectroscopy," J. Geophys. Res. **93,** 3851–3865 (1988).
21. M. M. Abbas, J. Guo, B. Carli, F. Mencaraglia, M. Carlotti, and I. G. Nolt, "Stratospheric distribution of HCN from far infrared observations," Geophys. Res. Lett. **14,** 531–534 (1987).
22. M. M. Abbas, J. Guo, B. Carli, F. Mencaraglia, M. Carlotti, and I. G. Nolt, "Heavy ozone distribution in the stratosphere from far infrared observations," J. Geophys. Res. **93,** 2063–2068 (1987).
23. M. Carlotti, A. Barbis, and B. Carli, "Stratospheric ozone vertical distribution from far infrared balloon spectra and statistical analysis of the errors," J. Geophys. Res. **94,** 16365–16372 (1989).
24. B. M. Dinelli, B. Carli, and M. Carlotti, "Measurement of stratospheric distribution of $H_2{}^{16}O$, $H_2{}^{18}O$, $H_2{}^{17}O$, and $HD^{16}O$ from far infrared spectra," J. Geophys. Res. **96,** 7509–7514 (1991).
25. M. M. Abbas, M. J. Glenn, I. G. Nolt, B. Carli, F. Mencaraglia, and M. Carlotti, "Far infrared measurements of stratospheric carbon monoxide," Geophys. Res. Lett. **15,** 140–143 (1988).
26. J. H. Park and B. Carli, "Spectroscopic detection of HO_2, H_2O_2 and OH in the stratosphere," J. Geophys. Res. **96,** 22535–22541 (1991).
27. D. H. Martin and E. Puplett, "Polarised interferometric spectrometry for the millimetre and submillimetre spectrum," Infrared Phys. **10,** 105–109 (1969).
28. D. H. Martin, "Polarizing (Martin–Puplett) interferometric spectrometers for millimeter and submillimeter spectra," in *Infrared and Millimeter Waves*, K. J. Button, ed. (Academic, 1982), Vol. 6, pp. 65–148.
29. B. Carli, P. A. R. Ade, U. Cortesi, P. Dickinson, M. Epifani, F. C. Gannaway, A. Gignoli, C. Keim, C. Lee, J. Leotin, F. Mencaraglia, A. G. Murray, I. G. Nolt, and M. Ridolfi, "SAFIRE/A—Spectroscopy of the Atmosphere using Far-Infrared Emission/Airborne," J. Atmos. Ocean. Technol. **16,** 1313–1328 (1999).
30. G. Bianchini, U. Cortesi, L. Palchetti, and E. Pascale, "SAFIRE/A (Spectroscopy of the Atmosphere by Far-Infrared Emission—Airborne): Optimized instrument configuration and new assessment of spectroscopic performances," Appl. Opt. **43,** 962–965 (2004).
31. G. Bianchini, M. Lanfranchi, and U. Cortesi, "Flight qualification of a diode laser for path difference determination of a high-resolution Fourier transform spectrometer," Appl. Opt. **39,** 962–965 (2000).
32. A. J. Viterbi, "Error bounds for convolution codes and an asymptotically optimum decoding algorithm," IEEE Trans. Inf. Theory **IT-13,** 260–269 (1967).
33. A. Boscaleri, V. Venturi, A. Tronconi, and R. Colzi, "A time

domain design technique for high precision full digital pointing system in balloon-borne remote infrared sensing," in *Acquisition, Tracking, and Printing IV*, Proc. SPIE **1304,** 127–136 (1990).
34. A. Boscaleri, V. Venturi, and R. Colzi, "A time domain computer simulation program as first step of a full digital high precision pointing system for platform in balloon-borne remote sensing," in *Infrared Technology XVI*, Proc. SPIE **1341,** 58–65 (1990).
35. A. Boscaleri, V. Venturi, and D. Tirelli, "The ARGO experiment pointing system as an example for other single axis platform pointing systems," Meas. Sci. Technol. **5,** 190–196 (1994).
36. L. M. Coyle, G. Aurilio, G. U. Nystrom, J. Bortz, B. G. Nagy, K. V. Chance, and W. A. Traub, "Design of a single-axis platform for balloon-borne remote sensing," Rev. Sci. Instrum. **57,** 2512–2518 (1986).
37. W. A. Traub, K. V. Chance, and L. M. Coyle, "Performance of a single-axis platform for balloon-borne remote sensing," Rev. Sci. Instrum. **57,** 2519–2522 (1986).
AQ: F 38. A. Murk, N. Kampfer, and N. J. Keen, "Baseline measurements with a 650 GHz radiometer," in *Proceedings of the Second Workshop on Millimetre Wave Technology and Application: Antennas*, Circuits and Systems, (1998), pp. 121–126.
AQ: G 39. A. S. Zachor, I. Coleman, and W. G. Mankin, "Effects of drive nonlinearities in Fourier spectroscopy," in *Spectrometric Techniques* (Academic, 1981), Vol. II.
40. L. Palchetti and D. Lastrucci, "Spectral noise due to sampling errors in Fourier transform spectroscopy," Appl. Opt. **40,** 3235–3243 (2001).
41. G. Bianchini and P. Raspollini, "Characterisation of instrumental line shape distortions due to path difference dependent phase errors in a Fourier transform spectrometer," Infrared Phys. Technol. **41,** 287–292 (2000).
42. A. S. Zachor and S. M. Aaronson, "Delay compensation: Its effect in reducing sampling errors in Fourier spectroscopy," Appl. Opt. **18,** 68–75 (1979).
43. B. Carli, A. Forni, and F. Mencaraglia, "Phase error correction in FT spectroscopy of spectra with positive and negative intensities," Int. J. Infrared Millim. Waves **3,** 529–540 (1982).
44. G. Bianchini, U. Cortesi, L. Palchetti, and E. Pascale, "Cosmic ray spikes localization and correction in FT spectrometer data," Infrared Phys. Technol. **43,** 33–38 (2002).
45. B. Carli, L. Palchetti, and P. Raspollini, "Effect of beamsplitter emission in Fourier-transform emission spectroscopy," Appl. Opt. **38,** 7475–7480 (1999).
46. B. Carli, F. Mencaraglia, A. Bonetti, M. Carlotti, and I. G. Nolt, "Detection of atomic oxygen and further line assignments in the far infrared atmospheric spectrum," Int. J. Infrared Millim. Waves **6,** 149–176 (1985).
47. J. H. Park and B. Carli, "Analysis of far-infrared emission Fourier transform spectra," Appl. Opt. **25,** 3490–3501 (1986).
48. M. Carlotti and B. Carli, "Approach to the design and data analysis of a limb-scanning experiment," Appl. Opt. **33,** 3237–3249 (1994).
49. M. Carlotti, "Global-fit approach to the analysis of limb-scanning atmospheric measurements," Appl. Opt. **27,** 3250–3254 (1988).
50. M. Ridolfi, B. Carli, M. Carlotti, T. von Clarmann, B. M. Dinelli, A. Dudhia, J.-M. Flaud, M. Höpfner, P. E. Morris, P. Raspollini, G. Stiller, and R. J. Wells, "Optimized forward model and retrieval scheme for MIPAS near-real-time data processing," Appl. Opt. **39,** 1323–1340 (2000).
51. F. Mencaraglia, G. Bianchini, A. Boscaleri, B. Carli, S. Ceccherini, J.-M. Flaud, and A. Perrin, "Comparison of rotational and vibrational spectroscopic data of HNO_3 for the validation of MIPAS satellite measurements," submitted to J. Geophys. Res. (2005). AQ: H
52. F. Friedl-Vallon, G. Maucher, M. Seefeldner, O. Trieschmann, A. Kleinert, A. Lengel, C. Keim, H. Oelhaf, and H. Fischer, "Design and characterization of the balloon-borne Michelson Interferometer for Passive Atmospheric Sounding (MIPAS-B2)," Appl. Opt. **43,** 3335–3355 (2004).
53. Y. Té, P. Jeseck, C. Camy-Peyret, S. Payan, G. Perron, and G. Aubertin, "Balloonborne calibrated spectroradiometer for atmospheric nadir sounding," Appl. Opt. **41,** 6431–6441 (2002).
54. D. G. Johnson, K. W. Jucks, W. A. Traub, and K. V. Chance, "Smithsonian stratospheric far infrared spectrometer and data reduction system," J. Geophys. Res. **100,** 3091–3106 (1995).
55. K. Strong, D. Barton, P. Bernath, S. Brown, J. Davies, J. R. Drummond, H. Fast, E. Farahani, P. Fogal, F. Goutail, J.-P. Goutail, R. Hall, J. C. McConnell, C. T. McElroy, S. M. L. Melo, C. Midwinter, F. Murcray, C. Nowlan, A. Ogyu, J. Olson, B. M. Quine, Y. Rochon, T. G. Shepherd, B. H. Solheim, D. Sommerfeldt, R. Sullivan, M. Tingley, M. Toohey, K. Walker, D. I. Wardle, H. Wu, D. Wunch, D. Tarasick, and A. Ullberg, "The MANTRA 2002 balloon flight from Vanscoy, Canada," presented at Envisat Validation Workshop, Frascati, Italy, 9–13 December 2002.